Visualization of Detergent Solubilization of Membranes: Implications for the Isolation of Rafts

Ashley E. Garner,* D. Alastair Smith,† and Nigel M. Hooper*
*Institute of Molecular and Cellular Biology and Leeds Institute of Genetics, Health and Therapeutics, and †Institute of Molecular Biophysics and the Astbury Centre for Structural Molecular Biology, University of Leeds, Leeds LS2 9JT, United Kingdom

ABSTRACT Although different detergents can give rise to detergent-resistant membranes of different composition, it is unclear whether this represents domain heterogeneity in the original membrane. We compared the mechanism of action of five detergents on supported lipid bilayers composed of equimolar sphingomyelin, cholesterol, and dioleoylphosphatidylcholine imaged by atomic force microscopy, and on raft and nonraft marker proteins in live cells imaged by confocal microscopy. There was a marked correlation between the detergent solubilization of the cell membrane and that of the supported lipid bilayers. In both systems Triton X-100 and CHAPS (3-[(3-cholamidopropyl)dimethylammonio]-1-propanesulfonate) distinguished between the nonraft liquid-disordered (l_d) and raft liquid ordered (l_o) lipid phases by selectively solubilizing the l_d phase. A higher concentration of Lubrol was required, and not all the l_d phase was solubilized. The solubilization by Brij 96 occurred by a two-stage mechanism that initially resulted in the solubilization of some l_d phase and then progressed to the solubilization of both l_d and l_o phases simultaneously. Octyl glucoside simultaneously solubilized both l_o and l_d phases. These data show that the mechanism of membrane solubilization is unique to an individual detergent. Our observations have significant implications for using different detergents to isolate membrane rafts from biological systems.

INTRODUCTION

Membrane rafts have been defined recently (1,2) as ''small (10–200 nm), heterogeneous, highly dynamic, sterol- and sphingolipid-enriched domains that compartmentalize cellular processes. Small rafts can sometimes be stabilized to form larger platforms through protein-protein and protein-lipid interactions''. These membrane microdomains have been implicated in the compartmentalization of a range of cellular processes, including intracellular trafficking, transmembrane signaling, lipid and protein sorting, viral uptake, and regulated proteolysis (3,4). In artificial model membranes, the tightly packed nature of the saturated acyl chains of the sphingolipids and their preferential interaction with cholesterol appear to render these lipid domains more resistant to solubilization by certain detergents than are the loosely packed unsaturated acyl chains of the glycerophospholipids in the surrounding bilayer (5). As a consequence numerous studies investigating rafts have relied upon this detergent resistance to isolate and characterize these membrane domains (detergent-resistant membranes; DRMs). However, it has been argued that detergent resistance is an artificial and highly subjective approach that can induce the formation of membrane domains and hence does not provide physiologically relevant information (1,6); and the assumption that detergents can isolate rafts in their native form has been heavily criticized (7,8). However, in the absence of direct experimental evidence comparing the mechanisms of detergent solubilization of cellular and model membranes, such conclusions may be considered premature.

One of the major concerns regarding the use of detergents to isolate rafts is that the DRMs may not represent preexisting domains. Investigations into the mechanism of detergent solubilization have revealed that the partitioning of detergent monomers into a membrane can induce phase separation and thereby create DRMs as a biochemical artifact (7,9). Detergents may also cause the aggregation of lipids and proteins which were in distinct membrane regions before detergent solubilization (10–12). Such findings not only raise questions about the relationship between membrane rafts and DRMs but also challenge whether rafts exist as phase-separated lipid domains in vivo.

It has been suggested that the composition of DRMs is dependent more upon solubilization dynamics than upon the arrangement of lipids and proteins in membrane domains and, therefore, that DRMs are unlikely to accurately represent the composition of membrane rafts (7,8,13). An alternative theory is that heterogeneous populations of rafts coexist within biological membranes and that certain preparation conditions favor the isolation of one or more of these raft species (10,14,15). For example, Triton X-100 (TX100) and 3-[(3-cholamidopropyl)dimethylammonio]-1-propanesulfonate (CHAPS) have been shown to isolate DRMs of a similar composition, whereas Lubrol and Brij 96 have been reported to isolate distinct raft populations that differ in their lipid and protein composition (10,14,16,17). However, there is no direct evidence to support the idea that different classes of rafts are isolated by different detergents (18). Unlike these other detergents, *n*-octyl-β-D-glucopyranoside (OG) is effective at rapidly solubilizing the whole membrane and is therefore

Submitted June 1, 2007, and accepted for publication September 17, 2007.

Address reprint requests to Nigel M. Hooper, Tel.: 44-113-343-3163; Fax: 44-113-343-6603; E-mail: n.m.hooper@leeds.ac.uk.

Editor: Petra Schwille.

0006-3495/08/02/1326/15 $2.00

doi: 10.1529/biophysj.107.114108

commonly used to solubilize lipid rafts and their associated proteins (19–21).

To elucidate the relationship between DRMs and physiological membrane rafts, a better understanding of the mechanisms involved in the detergent solubilization of cellular and model membranes is required. Atomic force microscopy (AFM) offers a unique approach to directly visualize the effects of detergent solubilization on lipid bilayers in real time. This technique has the added advantage of distinguishing between the raft-like, liquid-ordered (l_o) and nonraft, liquid-disordered (l_d) phases (22,23), allowing selective solubilization of specific phases to be monitored (24,25). However, high resolution AFM visualization of lipid phases is limited to model bilayers as imaging of the plasma membrane of live cells is hindered by the complex array of proteins and carbohydrates on the cell surface (26). Confocal microscopy provides an alternative approach to monitor the solubilization of live cells in real time using fluorescently tagged proteins as raft and nonraft markers (27,28). Several studies have used a glycosylphosphatidylinositol (GPI)-anchored form of a fluorescent protein (e.g., GPI-cyan fluorescent protein; GPI-CFP) to investigate rafts in mammalian cells and have found that these proteins are colocalized in rafts with other raft markers and are resistant to solubilization by TX100 (27–31). Conversely, the transmembrane protein vesicular stomatitis virus G (VSVG) fused to a fluorescent protein (e.g., VSVG-yellow fluorescent protein; VSVG-YFP) was excluded from raft domains and solubilized by TX100 (27,28). By using AFM of phase-separated supported lipid bilayers (SLBs) and confocal microscopy of live Chinese hamster ovary (CHO) cells coexpressing GPI-CFP and VSVG-YFP, we investigated the mechanism of solubilization of the raft-containing model and biological membranes by a range of detergents.

MATERIALS AND METHODS

Formation of supported lipid bilayers

Equimolar mixtures of egg sphingomyelin (Avanti Polar Lipids, Alabaster, AL), dioleoylphosphatidylcholine (DOPC), and cholesterol (both Sigma-Aldrich, Poole, UK) were prepared in chloroform/methanol (3:1 v/v) and dried under argon for 120 min. The dried lipid mixtures were rehydrated in Hepes-buffered saline (HBS; 50 mM Hepes/NaOH, 100 mM NaCl, pH 7.6) to a concentration of 2 mg/ml, vortexed to resuspend the lipid, and then sonicated at 60°C for 60 min to form lipid vesicles. The lipid vesicle sample was left to cool to room temperature before being used to form SLBs. The SLBs were prepared at room temperature (maintained at 23°C) by a vesicle fusion method adapted from Saslowsky et al. (32), which entailed transferring 10 μl of lipid vesicle sample onto freshly cleaved mica followed by 80 μl HBS containing 2 mM $CaCl_2$. After 3 min the SLB was washed three times with HBS, and a final volume of 100 μl of HBS was added to the SLB before imaging by AFM.

AFM imaging of supported lipid bilayers

AFM images were produced using a Digital Instruments Multimode atomic force microscope with a Nanoscope IIIa controller (Veeco, Santa Barbara, CA) equipped with an E-scanner (~14 μm^2 scan area). The scanner was calibrated according to Digital Instruments's standard procedures. AFM images of SLBs in aqueous buffer supported on stainless steel disks and mica sheets (Agar Scientific, Stansted, UK) using a fluid cell from Digital Instruments were recorded in tapping mode using oxide-sharpened, silicon nitride tips mounted on cantilevers with nominal spring constants of 0.32 Newton/m (Olympus, Tokyo, Japan), oscillating at a frequency between 7 and 9 KHz. The set point was adjusted during imaging to minimize the force while scanning at a rate of 1–2 Hz. Nanoscope offline software was used to flatten the AFM images, measure height differences, and estimate surface areas. AFM force measurements were used to plot force verses distance curves using the Nanoscope software.

Detergent solubilization of supported lipid bilayers

Solutions of Brij 96, TX100, and OG (Sigma-Aldrich), Lubrol 17A17 (Universal Biologicals, Cambridge, UK), and CHAPS (ICN Pharmaceutical, Hampshire, UK) were prepared in HBS. SLBs, which had been formed and washed in HBS, were imaged by AFM in tapping mode to obtain an image of the SLB at time zero, before the addition of detergent at room temperature (maintained at 23°C by air conditioning). The AFM scanner was then detached from the AFM to access the SLB and remove all of the HBS from the surface. The buffer was replaced with 100 μl of the appropriate detergent solution and the scanner reconnected. The SLB was then continuously imaged by AFM for 60 min to monitor the detergent extraction process in real time. To investigate the mechanisms of SLB solubilization and to facilitate comparisons between detergents, three detergent concentrations were studied, which corresponded to 1×, 3×, and 5× the critical micellar concentration (cmc) of the specific detergent (Table 1). To allow comparisons by absolute concentration, each detergent was also studied at a fourth concentration of 0.1%.

Plasmid DNA transfection of CHO cells

Complementary DNAs encoding GPI-CFP and VSVG-YFP were gifts from Dr. B. Nichols (MRC Laboratory of Molecular Biology, Cambridge, UK) and Dr. J. Lippincott-Schwartz (National Institutes of Health, Bethesda, MD), respectively. Transient transfections of GPI-CFP and VSVG-YFP plasmid DNA were performed using Lipofectamine 2000 (Invitrogen, Paisley, UK) according to the manufacturer's instructions. CHO cells were grown in antibiotic-free Ham's F12 medium.

Multifluorescent confocal microscopy

Confocal microscopy was performed on a Zeiss LSM 510 META equipped with an Axiovert 200 M inverted confocal microscope (Carl Zeiss, Hertfordshire, UK). A Plan-Neofluar 40×/1.3 oil differential interference contrast objective was used, and the multifluorescence imaging of GPI-CFP and VSVG-YFP in live CHO cells was achieved using multitracking scanning with Argon 458 nm and 514 nm excitation lasers. Emissions were separated by a main dichroic beam splitter HaupFarbTeiler 458/514 and a secondary dichroic beam splitter NebenFarbTeiler 490. The GPI-CFP signal was detected after a 480–520 nm band-pass filter with blocked infrared (IR); VSVG-YFP was detected after a 535–590 nm band-pass filter with blocked IR. Preliminary experiments involving successive additions of detergent were used to identify appropriate detergent concentrations for optimum visualization of this solubilization process within the 3 min imaging timeframe at 23°C.

RESULTS

Atomic force microscopy of phase-separated SLBs

To investigate whether detergents are capable of distinguishing between l_o and l_d phases, we used a system (equimolar

TABLE 1 Structures and properties of the detergents used in this study

Detergent	Structure	mw	cmc (mM)	cmc (%w/v)
TX100	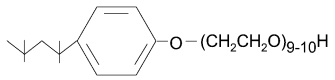	625	0.23	0.015
Lubrol	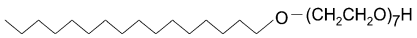	663	0.125	0.008
Brij 96	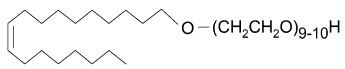	710	0.41	0.029
CHAPS	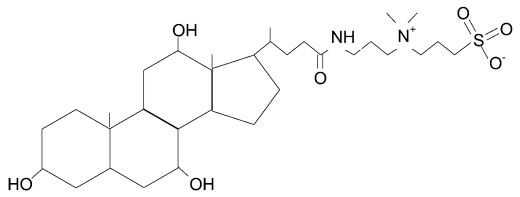	615	6.0	0.37
OG	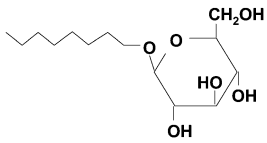	262	24.1	0.70

Data provided by the respective manufacturers.

sphingomyelin, DOPC, and cholesterol) that exhibits strong l_o/l_d phase separation. An SLB formed from sonicated lipid vesicles of equimolar sphingomyelin, DOPC, and cholesterol was imaged for 60 min by AFM and observed for any changes in domain morphology (Supplementary Fig. S1 *A*). As described previously (23,24,32), upon formation the SLB exhibited phase separation with rounded l_o domains protruding ~0.7 nm from the surrounding l_d phase. Over 60 min the total number of l_o domains gradually decreased, and their average size increased due to lipid lateral diffusion and domain coalescence. However, there was no net change in the surface area of the l_o phase (Supplementary Fig. S1 *B*), and the height difference between the two phases remained constant at 0.7 nm, indicating that the composition of each phase did not alter with time.

Confocal microscopy of CHO cells expressing fluorescent proteins

Confocal microscopy of CHO cells expressing GPI-CFP, VSVG-YFP, or both proteins revealed that the two different fluorescent proteins could be clearly differentiated and that there was no cross-contamination of fluorescence from either protein (Supplementary Fig. S2). Both GPI-CFP and VSVG-YFP were detected primarily at the cell surface. Distinct domains of either protein were not observed in cells coexpressing both proteins, in agreement with previous studies (27,28), probably due to the insufficient resolution of this microscopic approach. To determine whether photobleaching of the fluorescent proteins occurred during repetitive imaging, CHO cells expressing both GPI-CFP and VSVG-YFP were imaged every 4 s for 3 min. Minimal (<5%) photobleaching of GPI-CFP and VSVG-YFP was observed over this time period (Supplementary Fig. S3).

Solubilization of SLBs and CHO cells by Triton X-100

To investigate the mechanism of solubilization by TX100, AFM images were obtained at set time points after the addition of a range of concentrations of detergent to phase-separated SLBs. The addition of 0.015% (1× cmc) TX100 did not cause any solubilization of the SLB over 60 min (Fig. 1 *A*), and the changes in l_o domain morphology were similar to those observed in the control experiment in the absence of detergent (Supplementary Fig. S1); the total surface area in the l_o phase also remained unchanged (Fig. 1 *B*). However, alterations in the lipid packing were indicated by an immediate increase in height difference between the two phases from 0.69 nm to 1.06 nm upon detergent addition, probably

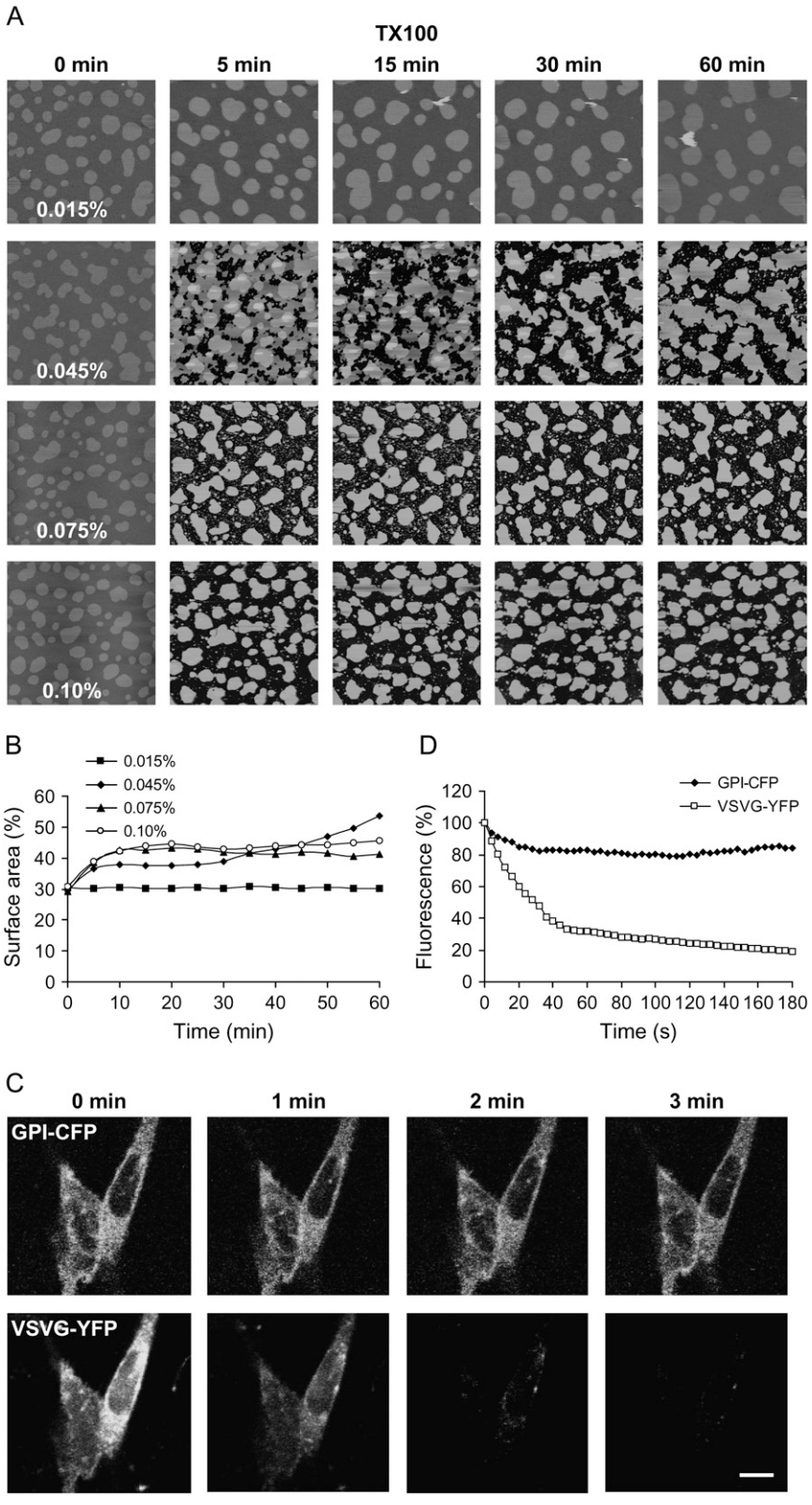

FIGURE 1 Solubilization of SLBs and CHO cells by TX100. (*A*) AFM images of SLBs at five time points over 60 min after the addition of 0.015%, 0.045%, 0.075%, or 0.1% TX100. At 0.015% TX100, no solubilization of the SLB occurs. Solubilization of the l_d phase begins after 5 min at 0.045% TX100, as indicated by the dark regions in the AFM image. After 30 min at 0.045%, solubilization of the l_d phase is complete but the l_o phase remains TX100 resistant. At 0.075% and 0.1% TX100, complete solubilization of the l_d phase occurs within 5 min, and the l_o domains are still resistant to solubilization after 60 min. Images are 10 μm scans with 10 nm height scale. (*B*) The surface area in the l_o phase as a percentage of the total area was determined for each AFM image after the addition of the indicated concentration of TX100 to SLBs. (*C*) CHO cells coexpressing GPI-CFP and VSVG-YFP were imaged by confocal microscopy every 4 s for 3 min during solubilization by 0.05% TX100. In contrast to the rapidly solubilized VSVG-YFP, GPI-CFP exhibited relative resistance to TX100 solubilization. Bar = 10 μm. (*D*) Percentage of fluorescence from GPI-CFP and VSVG-YFP during solubilization of CHO cells with TX100 as in (*C*).

due to the initial insertion of detergent monomers into the lipid bilayer. A similar increase in the height difference between the two phases was also observed after the addition of 0.045% (3× cmc) TX100 to the SLB. At this concentration, solubilization of the l_d phase began almost immediately, as indicated by the dark areas in the AFM image after 5 min (Fig. 1 *A*). The holes formed in the SLB allowed the absolute heights of the lipid phases to be measured. In the absence of detergent, the l_o domains had an absolute height of 6.46 nm and the l_d regions had an absolute height of 5.78 nm, as determined by force distance curves (data not shown). After the addition of TX100, both phases demonstrated a reduction in height: to 5.72 nm and to 4.65 nm for the l_o and l_d phases, respectively. These measurements suggest either that the TX100 monomers are entering both lipid phases where they are having a disordering effect on the lipid packing or that the insertion of the TX100 into the l_d phase is altering the lipid composition of both phases by inducing a reequilibrium. The fact that the l_d phase exhibited a greater reduction in height (1.13 nm) compared to the l_o phase (0.74 nm) indicated that the addition of TX100 was more disruptive to the l_d phase, which was further evidenced by the selective solubilization of the l_d phase in successive images.

The resistance of the l_o domains to TX100 solubilization was also observed at 0.075% (5× cmc) and 0.1% (6.7× cmc), even though the l_d phase was completely solubilized within the first 5 min of adding the detergent. These results appear to support the concept that TX100 can be used to isolate l_o domains by the selective solubilization of l_d regions. However, the change in bilayer height observed upon the addition of TX100 suggests that some reorganization of the domains may have occurred. At 0.075% and 0.1% TX100, the surface area of the l_o phase initially increased from 30% to 42% within the first 10 min after detergent addition but then did not significantly alter over the remaining 50 min (Fig. 1 *B*). In contrast, at 0.045% TX100 the l_o surface area exhibited a smaller increase—from 29% to 37%—within the first 10 min, remaining this size until all the l_d phase was solubilized; then another gradual increase in the surface area of l_o was observed from 30–60 min. This second increase in l_o surface area resulted in the greatest l_o surface area: 53%. Examination of successive images revealed that this increase in area was due to the deposition of bilayer from the surrounding solution rather than to an expansion of the l_o domains already present (data not shown).

It has been commented that TX100 may induce or promote the formation of l_o domains in membranes that show no stable l_o domains (8). To address this, we examined the effect of TX100 on a lipid mixture representative of the outer leaflet of human erythrocyte plasma membrane (sphingomyelin/phosphatidylcholine/phosphatidylethanolamine/cholesterol, 2.7:2.5:1:4.9) (33,34) that did not display phase separation (Supplementary Fig. S4) and can therefore be used as a homogenous membrane model. The addition of 0.5% TX100 to these SLBs resulted in immediate phase separation into distinct l_o and l_d domains, which differed in height by ~1.07 nm (Supplementary Fig. S4). After 30 min, the whole of the lower l_d phase was then solubilized (Supplementary Fig. S4) in a manner similar to that seen in the SLBs made from sphingomyelin, DOPC, and cholesterol (Fig. 1).

The addition of 0.05% TX100 to the CHO cells resulted in an immediate loss of VSVG-YFP from the cell surface, as demonstrated by the 68% reduction of YFP fluorescence within the first minute (Fig. 1, *C* and *D*). In contrast, GPI-CFP was relatively resistant to TX100 solubilization, and only a small reduction (16%) in CFP fluorescence was observed over the 3 min (Fig. 1, *C* and *D*). This differential solubilization of GPI-CFP and VSVG-YFP by TX100 is in agreement with previous studies (27–31). These data support the theory that rafts exist in cell membranes as phase-separated l_o domains which are resistant to solubilization by TX100.

Solubilization of SLBs and CHO cells by Lubrol

No solubilization of SLBs was observed at 0.008% (1× cmc), 0.024% (3× cmc), or 0.04% (5× cmc) Lubrol after 60 min, and only small defects penetrating 1.5 nm into the bilayer were observed after the addition of 0.1% (12.5× cmc) Lubrol (Fig. 2 *A* and data not shown). Since these experiments did not reveal any information regarding the process by which Lubrol solubilizes phase-separated SLBs, a higher concentration of 0.4% (50× cmc) was also studied (Fig. 2 *A*). An increase in the height difference between the phases from 0.68 nm to 1.08 nm was observed immediately after the addition of Lubrol. Comparing the absolute heights of the respective lipid phases from the holes formed during solubilization at 0.4% Lubrol revealed that both phases exhibited a slight reduction in height, with the l_o phase decreasing from 6.46 nm to 6.22 nm and the l_d phase decreasing from 5.78 nm to 5.14 nm. The morphology of the l_o domains was drastically altered during the solubilization process, but the l_o surface area remained at 32% (Fig. 2 *B*), indicating that only the l_d phase was solubilized during the 60 min period.

The addition of 0.4% Lubrol had little effect on the CHO cells, and no significant change in fluorescence was recorded for either GPI-CFP or VSVG-YFP during the 3 min of imaging by confocal microscopy (data not shown). To visualize the process of CHO cell solubilization by Lubrol, a higher concentration of 0.45% was used. Although this concentration solubilized the majority of VSVG-YFP from the cell surface, the CHO cells became disfigured during the 3 min of imaging, signifying that the integrity of the cells had been damaged (Fig. 2, *C* and *D*). The confocal microscopy images suggested that the solubilization of the CHO cells by 0.45% Lubrol was initiated by the preferential solubilization of VSVG-YFP followed by disruption of the plasma membrane, the release of cell contents, and the gradual solubilization of GPI-CFP. This process of Lubrol solubilization is comparable to that observed in phase-separated SLBs at 0.4% Lubrol (Fig. 2 *A*). The rearrangement of l_o domains seen in the SLB may account for the loss of membrane integrity observed in the live cell experiments with this detergent.

Solubilization of SLBs and CHO cells by Brij 96

The addition of Brij 96 to the SLBs resulted in solubilization even at the lowest concentration of 0.029% (1× cmc), where solubilized regions of SLB were evident after 5 min (Fig. 3 *A*). An increase in the height difference between the phases from 0.68 nm to 1.06 nm occurred immediately after the addition of Brij 96, and determination of absolute phase heights at the solubilized edges revealed that both phases exhibited a

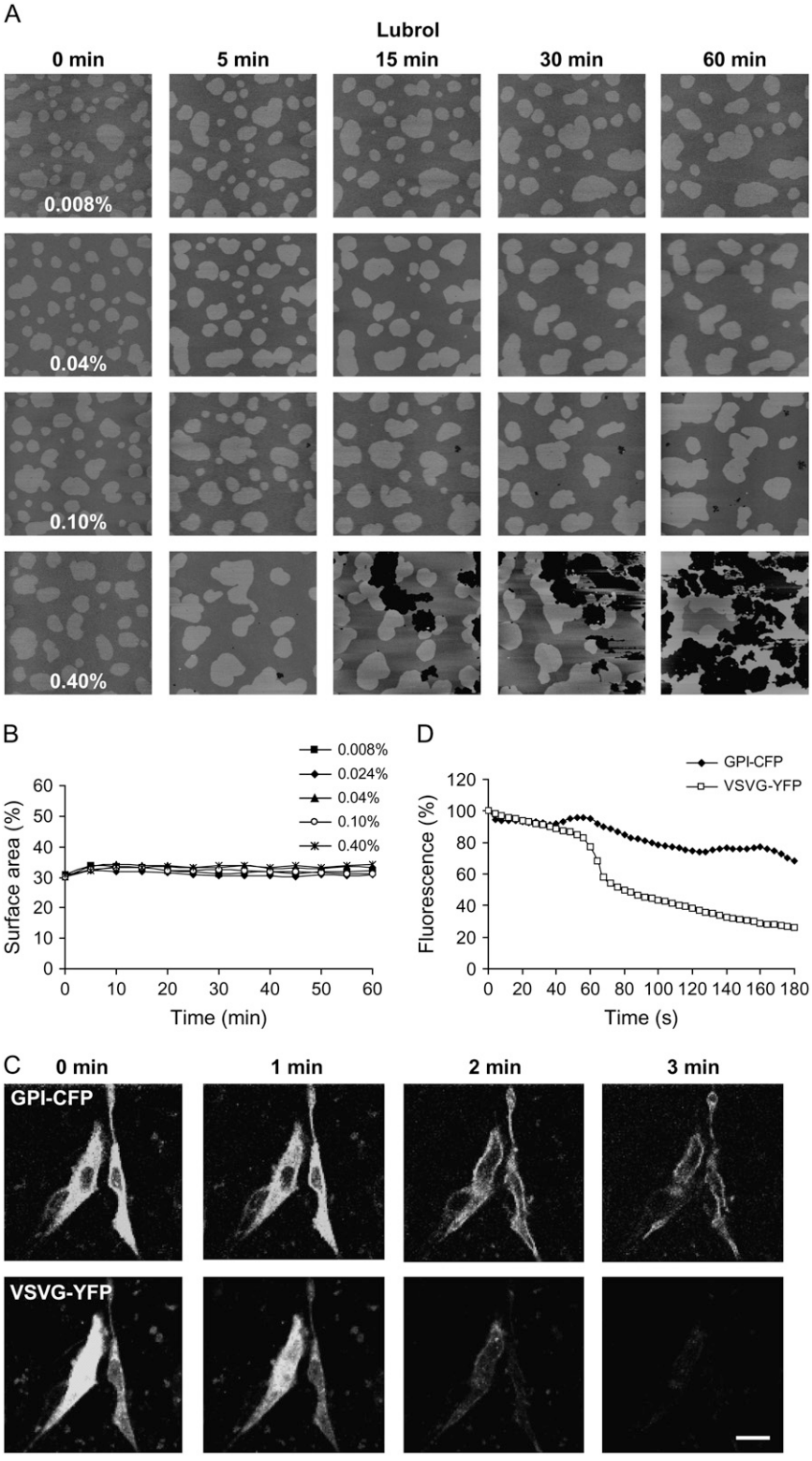

FIGURE 2 Solubilization of SLBs and CHO cells by Lubrol. (*A*) AFM images of SLBs at five time points over 60 min after the addition of 0.008%, 0.04%, 0.1%, or 0.4% Lubrol. No solubilization of the SLBs was observed at 0.008% or 0.04%, and only small holes began to form in the l_d phase at 0.1% Lubrol. The addition of 0.4% Lubrol resulted in extensive solubilization which predominately occurred at the interface between the l_d and l_o phases. Images are 10 μm scans with 10 nm height scale. (*B*) The surface area in the l_o phase as a percentage of the total area was determined for each AFM image after the addition of the indicated concentration of Lubrol to SLBs. (*C*) CHO cells coexpressing GPI-CFP and VSVG-YFP were imaged by confocal microscopy every 4 s for 3 min after the addition of 0.45% Lubrol. VSVG-YFP was preferentially solubilized initially, with GPI-CFP solubilization accompanying the loss of membrane integrity. Bar = 10 μm. (*D*) Percentage of fluorescence from GPI-CFP and VSVG-YFP during solubilization of CHO cells by 0.45% Lubrol as in (*C*).

reduction in height, with the l_o phase decreasing from 6.46 nm to 4.92 nm and the l_d phase from 5.78 nm to 3.86 nm. Although the difference in height between the phases was comparable after the addition of TX100 and Brij 96, the absolute heights of the respective phases were 0.8 nm lower with Brij 96, indicating a greater disruption to the bilayer lipid packing. The process of solubilization displayed by Brij 96 shared characteristics with that of TX100. The initial solubilization appeared to occur in the l_d phase, where holes started to form throughout the phase. This suggests that a threshold Brij 96 concentration has been achieved in the l_d phase in a manner similar to that observed for TX100. However, further solubilization of the SLB proceeded from holes that were formed at the interface between the phases. Whole 4 μm^2 patches of bilayer were solubilized in between consecutive images (i.e., within 5 min), implying that all the lipids in that area were being solubilized simultaneously.

In contrast to TX100, the addition of Brij 96 resulted in an initial decrease in l_o surface area except at 0.145% (5× cmc) (Fig. 3 *B*). A steady decrease in l_o surface area over 60 min was also observed at all concentrations of Brij 96, suggesting that some of the lipids from the l_o phase were being either redistributed into the l_d phase or solubilized by the Brij 96. It is feasible that the accumulation of Brij 96 at the lipid phase interface may facilitate the solubilization of some l_o phase in unison with the l_d phase. Rapid solubilization of the l_d phase was observed at 0.145% Brij 96, which was accompanied by a slight increase in l_o surface area initially. A gradual solubilization of the l_o phase then resulted in a diminishing l_o surface area over the 60 min, and additional images revealed that the whole SLB was solubilized within 90 min (data not shown). Again, large areas of bilayer from the edges of the domains were solubilized in unison, leaving characteristic crescent-shaped domains in their place. This suggests that Brij 96 can solubilize l_o domains from their exposed edges and supports the concept that accumulation at the phase interface could account for the solubilization of l_o domains observed at lower concentrations of Brij 96.

The addition of 0.075% Brij 96 to CHO cells coexpressing GPI-CFP and VSVG-YFP resulted in an immediate loss of VSVG-YFP from the cell surface, causing a 55% reduction in YFP fluorescence within the first minute (Fig. 3, *C* and *D*). In contrast, only a slight decrease (14%) in CFP fluorescence was observed during this time due to the loss of GPI-CFP. Continued solubilization of VSVG-YFP at a slower rate occurred over the next 2 min, whereas a sudden loss of GPI-CFP was observed at ~96 s, which was then followed by a more gradual reduction in CFP fluorescence (Fig. 3, *C* and *D*). The solubilization of GPI-CFP and VSVG-YFP by Brij 96 appeared to proceed by distinct mechanisms and, despite a significant loss of both proteins from the cell surface of CHO cells, a small proportion of both proteins still remained after 3 min. The process of Brij 96 solubilization observed in CHO cells was comparable to that displayed in phase-separated SLBs, where solubilization initially occurred in the l_d region followed by the instantaneous disappearance of larger l_o regions.

Solubilization of SLBs and CHO cells by CHAPS

At 0.1% CHAPS no solubilization of the SLB was detected (Fig. 4 *A*), but patches of higher regions characteristic of a second bilayer forming on top of the SLB were detected, suggesting that the detergent concentration was sufficient to cause reorganization but not solubilization of the SLB. Solubilization at 0.37% (1× cmc) CHAPS resulted in the rapid solubilization of the l_d phase accompanied by an initial increase in l_o surface area which remained resistant to solubilization over the course of the experiment (Fig. 4 *A*). At 1.11% (3× cmc) CHAPS the initial increase in l_o surface area was closely followed by a steep decline and then a more gradual loss as the l_o phase was solubilized (Fig. 4 *B*). The AFM images revealed that a large number of small l_o domains which remained after 5 min were solubilized in successive images and that the loss of these domains coincided with the steep decline in l_o surface area. The remaining domains appeared to get progressively smaller as if the outer edges were being gradually solubilized. This edge solubilization was distinct from that observed for Lubrol and Brij 96 since only small reductions in the domain size were visible in successive images with little alteration in domain shape. This suggests that CHAPS solubilization of the l_o phase was due to the gradual removal of edge lipids, which would also account for the loss of smaller domains before larger domains due to their greater perimeter/area ratio. At 1.85% (5× cmc) CHAPS the whole SLB was completely solubilized within 30 min. The AFM images and l_o surface area data indicate that the process of solubilization was similar to that observed at 1.11% CHAPS, with the initial solubilization of the l_d phase followed by the progressive loss of the l_o lipids from the edges of the remaining domains.

The addition of 0.5% CHAPS to CHO cells coexpressing GPI-CFP and VSVG-YFP resulted in the loss of the majority of the VSVG-YFP from the cell surface within the first minute (Fig. 4, *C* and *D*). A significant proportion of GPI-CFP was also solubilized immediately after the addition of CHAPS, as demonstrated by a 40% reduction in CFP fluorescence in the first minute (Fig. 4, *C* and *D*). The gradual loss of both proteins was observed over the remaining course of the experiment, and little VSVG-YFP was detectable in the confocal images after 2 min. In contrast, a small proportion of GPI-CFP was still visible after 3 min. These results suggest that GPI-CFP is slightly more resistant to CHAPS solubilization than is VSVG-YFP. This is in agreement with the data from the phase-separated SLBs, which revealed that the initial solubilization of l_d domains by CHAPS was frequently accompanied by a more gradual solubilization of the l_o phase.

Solubilization of SLBs and CHO cells by octyl glucoside

Some solubilization of the SLB was observed at 0.1% (0.14× cmc) OG, and the holes that formed were surrounded by higher areas, which were equivalent in height to the l_o

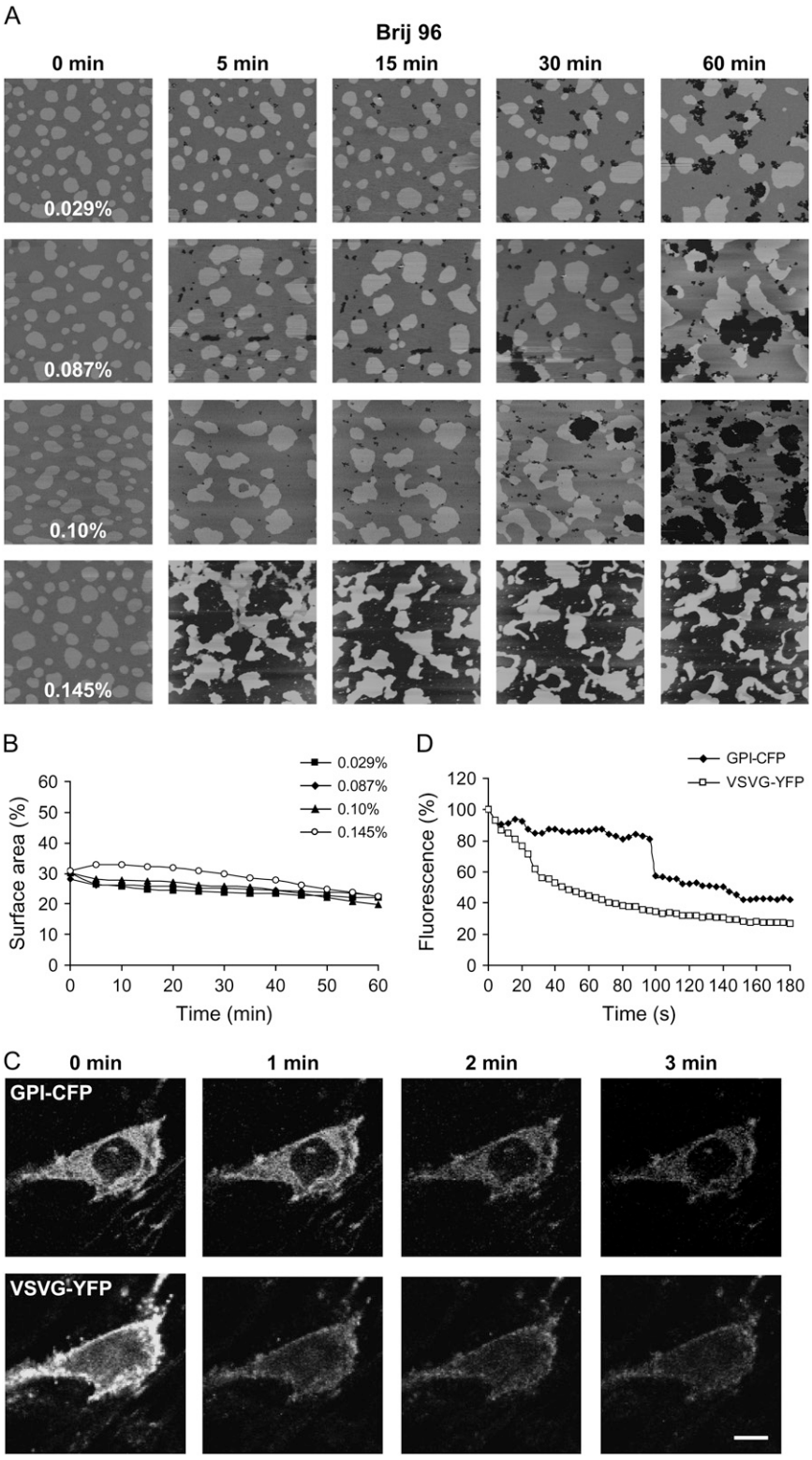

FIGURE 3 Solubilization of SLBs and CHO cells by Brij 96. (*A*) AFM images of SLBs at five time points over 60 min after the addition of 0.029%, 0.087%, 0.1%, or 0.145% Brij 96. Solubilization of the SLBs was observed at all concentrations and although holes originated in the l_d phase, progressive solubilization appears to occur at the interface between the l_d and l_o phase. Images are 10 μm scans with 10 nm height scale. (*B*) The surface area in the l_o phase as a percentage of the total area was determined for each AFM image after the addition of the indicated concentration of Brij 96 to SLBs. (*C*) CHO cells coexpressing GPI-CFP and VSVG-YFP were imaged by confocal microscopy every 4 s for 3 min after the addition of 0.075% Brij 96. Preferential solubilization of VSVG-YFP in the first minute was followed by GPI-CFP solubilization. A small proportion of both proteins remained after 3 min. Bar = 10 μm. (*D*) Percentage of fluorescence from GPI-CFP and VSVG-YFP during solubilization of CHO cells with 0.075% Brij 96 as in *C*.

domains (Fig. 5 *A*). However, it is not clear from the AFM images whether these higher areas surrounding the holes were preexisting l_o domains or were formed during the solubilization of the l_d phase. The dispersed appearance of these higher areas and the observed increase in l_o surface area (Fig. 5 *B*) suggest that they may have been formed from lipids in the l_d phase. Although the holes were observed immediately after the addition of 0.1% OG, they accounted for only 1% of the

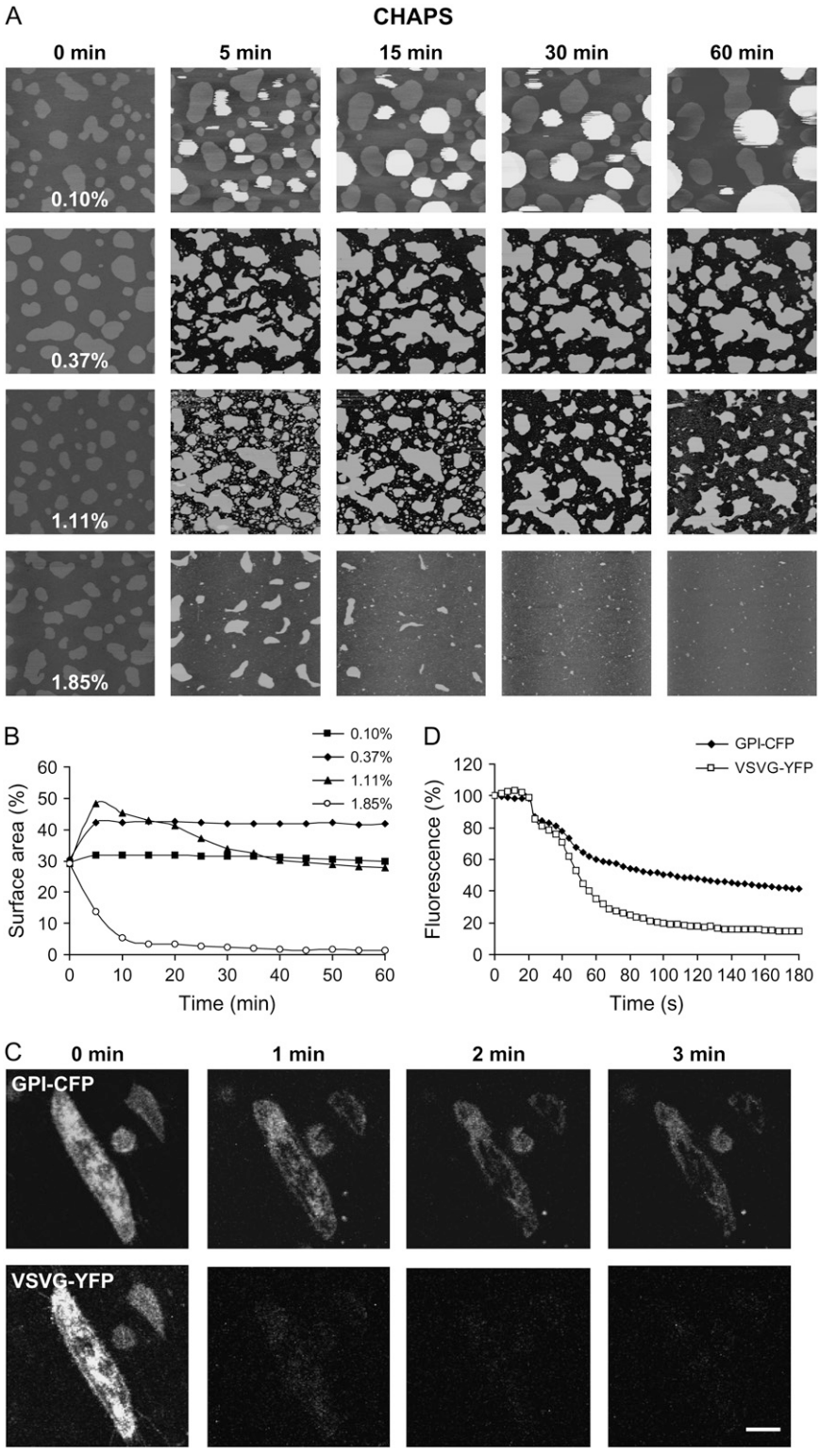

FIGURE 4 Solubilization of SLBs and CHO cells by CHAPS. (*A*) AFM images of SLBs at five time points over 60 min after the addition of 0.1%, 0.37%, 1.11%, or 1.85% CHAPS. No solubilization of the SLB was observed at 0.1%. Complete solubilization of the l_d phase was observed at 0.37%, whereas the l_o domains remained CHAPS resistant. At 1.11% CHAPS solubilization of the l_d phase was followed by progressive l_o solubilization, and at 1.85% CHAPS the whole SLB was solubilized within 30 min. Images are 10 μm scans with 10 nm height scale. (*B*) The surface area in the l_o phase as a percentage of the total area was determined for each AFM image after the addition of the indicated concentration of CHAPS to SLBs. (*C*) CHO cells coexpressing GPI-CFP and VSVG-YFP were imaged by confocal microscopy every 4 s for 3 min after the addition of 0.5% CHAPS. Significant loss of both proteins was observed, but GPI-CFP was comparatively more resistant to CHAPS solubilization. Bar = 10 μm. (*D*) Percentage of fluorescence from GPI-CFP and VSVG-YFP during solubilization of CHO cells with 0.5% CHAPS as in (*C*).

total surface area and little further solubilization occurred over the 60 min period.

To interpret the AFM images at 0.7% (1× cmc), 2.1% (3× cmc), and 3.5% (5× cmc) OG, force curves were used to determine whether a bilayer was still present in the featureless regions. A typical force curve of a lipid bilayer in the l_d phase showed contact with the tip 5.7 nm above the mica and the tip penetrated at a force of ~2 nN (Supplementary

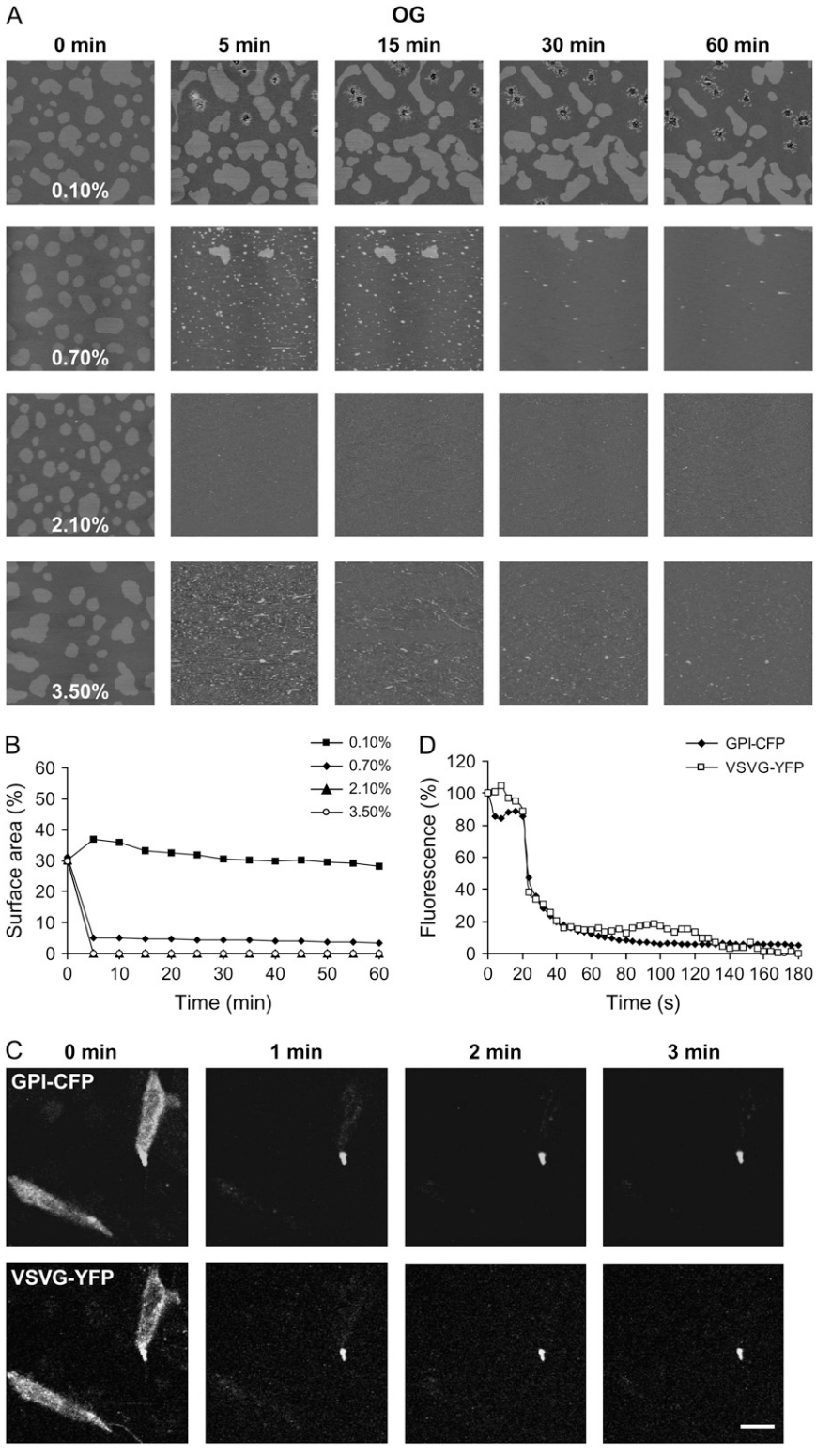

FIGURE 5 Solubilization of SLBs and CHO cells by OG. (*A*) AFM images of SLBs at five time points are shown after the addition of 0.1%, 0.7%, 2.1%, or 3.5% OG. Some small holes formed in the SLB at 0.1% OG but little solubilization occurred. All but two lipid domains were solubilized at 0.7% OG, and the whole SLB was solubilized within 5 min at 2.1% and 3.5% OG. Images are 10 μm scans with 10 nm height scale. (*B*) The surface area in the l_o phase as a percentage of the total area was determined for each AFM image after the addition of the indicated concentration of OG to SLBs. (*C*) CHO cells coexpressing GPI-CFP and VSVG-YFP were imaged by confocal microscopy every 4 s for 3 min after the addition of 0.75% OG. Considerable loss of both proteins from the cell surface was observed within 1 min. The bright fluorescent spot in subsequent images is contamination from a dead cell. Bar = 10 μm. (*D*) Percentage of fluorescence from GPI-CFP and VSVG-YFP during solubilization of CHO cells with 0.75% OG as in (*C*). To reflect the relative fluorescence of the live cells only, the bright spot of fluorescence observed in (*C*) was excluded.

Fig. S5 *A*). In contrast, force curves of the featureless regions in the OG AFM images indicated a slight resistance (~0.5 nN) 2 nm above the mica surface, which was not characteristic of a lipid bilayer (Supplementary Fig. S5 *B*). This suggests that the whole SLB had been solubilized by OG and the substance detected by the AFM probe probably represented some residual lipid/detergent aggregates. Therefore, at 0.7% OG, all the SLB was solubilized except for two domains and the

entire SLB was solubilized within 5 min at 2.1% and 3.5% OG.

The addition of 0.75% OG to CHO cells coexpressing GPI-CFP and VSVG-YFP resulted in a considerable loss of both GPI-CFP and VSVG-YFP during the first minute of imaging (Fig. 5, *C* and *D*). Although indiscriminate solubilization by OG appeared to account for the simultaneous rapid reduction of CFP and YFP fluorescence after 24 s, a slight decline in CFP fluorescence was also observed immediately preceding this rapid solubilization (Fig. 5 *D*), suggesting that the initial stages of OG solubilization may target raft domains. These data, supported by the findings from experiments in phase-separated SLBs, demonstrated a similar process of immediate solubilization of both lipid phases after the addition of OG.

DISCUSSION

In this study we investigated the mechanisms of solubilization by different detergents of phase-separated SLBs and compared these to the effects of the detergents on live CHO cells. The results from the experiments using AFM to visualize SLBs in real time revealed that each detergent solubilized the lipid bilayer by a different mechanism and that this influenced the nature of the domains that remained after detergent extraction. Interestingly, these same mechanisms were also evident during the detergent solubilization of CHO cells as determined by confocal microscopy using fluorescent raft and nonraft proteins. Although less insight is gained into the action of the detergents when the fluorescence data are analyzed in isolation, due to the lower resolution of the confocal microscope and the relatively rapid speed of solubilization required for visualization by this technique, when combined with the AFM data on phase-separated SLBs, consistencies in the apparent process of solubilization by the respective detergents are evident, providing significant and novel (to our knowledge) insight into the process of detergent solubilization of biological membranes. Furthermore, the similarities observed in the actions of the detergents on l_o domains in SLBs and on GPI-CFP in CHO cells support the theory that rafts exist as phase-separated domains in cellular membranes. However, the CHO cells were much more susceptible to detergent solubilization in comparison to the SLBs, even when the differences in detergent/lipid ratio were accounted for. Several studies have reported similar observations, and the most likely explanation is that the membrane proteins, especially those that traverse the whole bilayer, cause weaknesses in the membrane which facilitate detergent insertion and solubilization (35).

From the AFM images it can be seen that in the SLBs the l_o domains range from 1–3 μm in diameter, as compared to 10–200 nm for rafts in cell membranes (1). This difference in size is probably due to a number of factors and has been discussed in detail previously (36–38). For example, as cell membranes are more complex than model membranes, ordered lipid domains in cells may exist at the borderline of conditions at which they are stable, and/or in the form of almost infinitesimal nanodomains (38). In addition, both cholesterol and proteins, particularly if they preferentially localize to the edges of rafts, will reduce raft size. As the l_o domains in the SLBs are not equivalent in composition to rafts in cell membranes and are not under the same dynamic restraints, it is perhaps not surprising that they are larger. Indeed, if left for prolonged periods of time, the l_o domains in the SLBs move and fuse to form even larger domains (data not shown).

Comparing the mechanisms of solubilization by the different detergents

When the solubilization of SLBs was investigated over a range of detergent concentrations proportional to the cmc, a distinct process of detergent solubilization was observed for each detergent. Increasing the concentration of the detergent typically caused an increase in the rate or extent of solubilization, but the mechanism was found to be generally consistent over the range of concentrations investigated. These same mechanisms were also evident during the detergent solubilization of the CHO cells, which suggests that the DRMs isolated from cells are more dependent on the properties of the detergent than on the actual organization of lipids and proteins in cellular membranes. The resistance of l_o domains to TX100 solubilization observed in these experiments clearly indicates that TX100 can distinguish between the l_d and l_o lipid phases by selectively solubilizing the l_d phase. However, the resultant l_o domains may be contaminated with TX100 and/or additional lipids that originated from the l_d phase. Therefore, although domains isolated after TX100 solubilization will contain preexisting l_o domains, they may not entirely represent preexisting domains in their native state. In addition, it would appear that TX100 can promote domain formation in a membrane where phase separation does not preexist.

The mechanism of solubilization by 0.4% Lubrol was in contrast to that by TX100. For TX100 the whole l_d phase began to solubilize at once as if a critical concentration of detergent had been reached throughout the phase. In contrast, the solubilization by Lubrol grew outward from several areas where holes initially formed in the l_d phase, suggesting that solubilization was occurring from the exposed bilayer edges rather than from a buildup of Lubrol throughout the phase. The initial holes originated at the interface between the two phases, possibly indicating that a higher local concentration of Lubrol was accumulating in this area. It is feasible that the interface between the two phases was more susceptible to detergent insertion since neighboring lipids in opposing phases will be mismatched in height and lipid packing. It should also be noted that the concentration of Lubrol required to solubilize the bilayer was much higher than that of TX100, and even at 0.4% Lubrol some l_d phase still remained after

60 min, leading to the contamination of isolated Lubrol domains with l_d phase.

The solubilization of SLBs by Brij 96 appeared to occur by a two-stage mechanism that initially resulted in the solubilization of some l_d phase and then progressed to the solubilization of both l_d and l_o phases simultaneously, resulting in the isolation of partially solubilized l_d and l_o phases. This suggests that the threshold concentration required to initiate solubilization of the l_o phase is less than that required to completely solubilize the l_d phase. Confocal microscopy of the CHO cells revealed a similar process of solubilization as identified by the raft and nonraft marker proteins. The consequence of this mechanism of solubilization is that DRMs isolated by Brij 96 may potentially contain two different lipid environments, one which is analogous to a partially solubilized form of l_o domain and one which corresponds to incompletely solubilized l_d domain. Interestingly, characterization of Brij 96 DRMs isolated from neuronal cells revealed that these complexes contained two different ''microenvironments'' which differed in their lipid and protein composition (39). Other studies which have investigated the composition of Brij 96 DRMs have also reported that they are less enriched in SM and cholesterol, include more unsaturated lipids, and contain more proteins compared to DRMs isolated by TX100 or CHAPS (10,40,41). In addition, some proteins which were associated with TX100 DRMs were found to be solubilized by Brij 96 (10,41). All these features are consistent with the concept that Brij 96 DRMs contain partially solubilized l_o and l_d domains.

The mechanism of SLB solubilization exhibited by CHAPS was comparable to that of TX100 in a number of ways. As with TX100, preferential solubilization of the l_d phase was observed during CHAPS solubilization of the SLBs and, at the appropriate concentration (e.g., 0.37%), complete isolation of detergent-resistant l_o domains was demonstrated. An initial increase in the surface area of the l_o phase was also observed in CHAPS-solubilized SLBs, suggesting that, like TX100, CHAPS may alter the lipid packing or lateral organization of the lipid bilayer. Studies investigating the solubilization of cellular membranes by different detergents have also reported similarities in both the lipid and protein composition of DRMs isolated by TX100 and CHAPS (40,42). As the mechanism of CHAPS solubilization shared similarities with that of TX100, the same caveats apply regarding the increased surface area of isolated domains compared to preexisting l_o domains and the possible redistribution or aggregation of lipids. In addition, the gradual loss of lipids from domain edges could result in isolation of partially solubilized domains.

OG has been reported to solubilize lipid rafts and is therefore typically employed in cellular studies when solubilization of the whole membrane is required (19–21). The results of this study clearly demonstrate that OG is extremely efficient at causing instant and complete solubilization of both SLBs and CHO cells, possibly involving simultaneous solubilization of both l_o and l_d phases. Analysis of cellular lipids solubilized by increasing concentrations of OG revealed that, unlike other detergents, OG displayed little discrimination between lipid species and solubilized each lipid in comparable proportions (43). This suggests that OG solubilization affects the whole bilayer equally, regardless of the lipid composition.

Comparing detergents at the same concentration

The limitations of comparing detergents at a single absolute concentration presented here has important implications for studies that have directly compared the protein and lipid composition of DRMs from cells after treatment with different detergents at the same concentration. For example, comparing the solubilization of SLBs at the same concentration of Lubrol and TX100 revealed that very little solubilization of the SLB (<3%) was observed at 0.1% Lubrol, whereas 0.1% TX100 resulted in the extraction of over 50% of the SLB with complete solubilization of the l_d phase. One of the earliest studies to characterize Lubrol DRMs (14) found that the membrane protein prominin was solubilized by 0.5% TX100 but remained insoluble in 0.5% Lubrol. The authors suggested that distinct ''Lubrol rafts'' containing prominin coexisted with the ''TX100 rafts''. Further investigation revealed that the GPI-anchored, raft-associated placental alkaline phosphatase (PLAP) was associated with both Lubrol and TX100 DRMs. This suggested that the Lubrol DRMs contained some, if not all, of the TX100 DRMs; a variety of techniques were used to show that prominin and PLAP were in distinct microdomains on the cell surface. The authors concluded that their results supported the concept of multiple, distinct, coexisting raft domains which could be differentiated by different detergents. An alternative explanation for these results can be put forward on the basis of the observations in this study. Assuming the cell surface was phase separated into l_o raft domains and l_d nonraft domains, the treatment of the cells with equivalent concentrations of TX100 and Lubrol would result in the isolation of ''l_o rafts'' in the TX100 DRMs and ''l_o rafts plus incompletely solubilized l_d nonrafts'' in the Lubrol DRMs. The fact that PLAP was isolated in both TX100 and Lubrol DRMs agrees with PLAP being localized to the l_o raft domains. Accordingly, the observation that prominin was excluded from TX100 DRMs, but was present in Lubrol DRMs, could be explained if prominin is excluded from the l_o rafts and localized in the l_d nonraft domains. This would also explain why PLAP and prominin appeared to associate with different complexes within the Lubrol DRMs and occupy spatially distinct domains on the cell surface.

The fundamental implications of interpreting the results of Roper et al. (14) in accordance with the findings of this study are threefold. First, this would suggest that prominin is not localized in lipid rafts. Second, it implies that compositionally distinct rafts do not coexist within the same cellular membrane or at least that they are not distinguishable by their

differential solubility in TX100 and Lubrol. Third, it suggests that Lubrol may be ineffective at solubilizing the nonraft portion of cellular membranes at the concentrations typically used in extraction experiments, resulting in the isolation of DRMs which do not greatly differ from the bulk plasma membrane. In support of this third point, the transferrin receptor, which is not localized in rafts, has been isolated in Lubrol DRMs by several studies (11,40,44), supporting the concept that Lubrol DRMs still contain nonraft regions of the plasma membrane. Studies investigating the lipid composition of Lubrol DRMs have confirmed that Lubrol DRMs contain a higher proportion of unsaturated glycerophospholipids than do TX100 DRMs, although Lubrol DRMs still contain an equivalent amount of sphingolipids and saturated glycerophospholipids (11,16). Again, this is consistent with the Lubrol DRMs containing the equivalent TX100 DRMs in addition to some residual nonraft regions of the membrane.

Implications for using detergents to isolate membrane rafts

The results of this study reveal that some detergents, such as TX100 and CHAPS, do exhibit selective solubilization of the l_d lipid phase at appropriate concentrations. Lubrol, Brij 96, and OG were less discriminating, which resulted in the partial or complete solubilization of both lipid phases. This clearly indicates that although certain detergents have the ability to distinguish between the lipid phases—and so can be used to isolate raft domains—this is not a common property of all detergents. These results also indicate that the isolated detergent domains are unlikely to accurately represent raft domains in their native form. Compositional and structural changes of the l_o domains were detected after the addition of detergent, as indicated by the domain surface area and height measurements. This could be due to the incorporation of detergent monomers in the l_o phase, in which case the lipid and protein content of DRMs would still represent raft domains. Alternatively, if reorganization or reequilibration of the lipids between phases occurred upon detergent addition, the isolated domains could differ dramatically in lipid and protein composition from the preexisting raft domains.

Even if the physical changes (i.e., height) of the lipid bilayer observed in this study could be attributed to the incorporation of detergent into the bilayer, DRMs would still be susceptible to the overestimation or underestimation of raft domains. If the detergent concentration was too low (in relation to the lipid concentration) or if the extraction time was too short, overestimation of raft domains would occur, resulting in the incomplete solubilization of the l_d phase as observed for 0.4% Lubrol after 60 min or 0.045% TX100 after 5 min. If the detergent concentration was too high (in relation to the lipid concentration) or if the extraction time was too long, underestimation of raft domains would occur, resulting in partial solubilization of the l_o phase as observed for 1.11% and 1.85% CHAPS.

This study clearly demonstrates that DRMs of varying compositions can be isolated from the same initial phase-separated SLB by different detergents. For example, 45% of the SLB surface area remained after 60 min with 0.1% TX100, all of which was in the l_o phase. In contrast, 55% of the SLB surface area remained after 60 min with 0.1% Brij 96, and only 19% of this was in the l_o phase. Without the AFM images to visualize the solubilization process, such results could be interpreted as the isolation of different domain populations by the specific detergents. In addition, variation in DRM compositions could also occur due to the partial solubilization of l_d or l_o domains, resulting in overestimation or underestimation of raft domains by different detergents. This may be especially applicable to detergents that, like Lubrol, require high concentrations to completely solubilize the l_d phase and are therefore susceptible to overestimating raft domains.

CONCLUSIONS

Our results show that even under the assumptions that rafts are present in cellular membranes, are comparable to the l_o domains of SLBs, and are more resistant to detergent solubilization than the remainder of the membrane, the use of detergents to isolate rafts requires considerable caution. As demonstrated for both SLBs and CHO cells, detergent solubilization is a dynamic process dependent upon the extraction time as well as the concentration and nature of the detergent used. To determine when the l_d nonraft regions have been completely solubilized and the l_o raft domains are preserved in their entirety requires that the process be visualized in real time. In the absence of suitable technology to allow such routine visualization, it will remain difficult to isolate membrane rafts from live cells in their native form using detergents. The fact that the detergent-specific mechanisms of solubilization demonstrated in SLBs were also observed in cellular membranes has significant implications for studies on DRMs isolated by different detergents. Several studies (e.g., 10,14) have reported the isolation of unique DRMs by Lubrol and Brij detergents, which has led to the hypothesis that distinct populations of rafts coexist in cellular membranes. However, the results of this study suggest that such variation may be attributable more to the unique properties of the individual detergents than to the actual raft domains.

SUPPLEMENTARY MATERIAL

To view all of the supplemental files associated with this article, visit www.biophysj.org.

We thank Dr. S. Connell for assistance with the AFM and Dr. G. Howell for assistance with the confocal microscopy.

A.E.G. received a studentship from the Biotechnology and Biological Sciences Research Council (BBSRC) of Great Britain. The financial support of the BBSRC, the Medical Research Council of Great Britain, and the Wellcome Trust (Bioimaging Facility, University of Leeds) is gratefully acknowledged.

REFERENCES

1. Pike, L. J. 2006. Rafts defined: a report on the Keystone symposium on lipid rafts and cell function. *J. Lipid Res.* 47:1597–1598.
2. Jacobson, K., O. G. Mouritsen, and R. G. Anderson. 2007. Lipid rafts: at a crossroad between cell biology and physics. *Nat. Cell Biol.* 9:7–14.
3. Hooper, N. M. 1999. Detergent-insoluble glycosphingolipid/cholesterol-rich membrane domains, lipid rafts and caveolae. *Mol. Membr. Biol.* 16: 145–156.
4. Simons, K., and D. Toomre. 2000. Lipid rafts and signal transduction. *Nat. Rev. Mol. Cell Biol.* 1:31–39.
5. Brown, D. A., and E. London. 1998. Structure and origin of ordered lipid domains in biological membranes. *J. Membr. Biol.* 164:103–114.
6. Shogomori, H., and D. A. Brown. 2003. Use of detergents to study membrane rafts: the good, the bad, and the ugly. *Biol. Chem.* 384:1259–1263.
7. Heerklotz, H. 2002. Triton promotes domain formation in lipid raft mixtures. *Biophys. J.* 83:2693–2701.
8. Lichtenberg, D., F. M. Goni, and H. Heerklotz. 2005. Detergent-resistant membranes should not be identified with membrane rafts. *Trends Biochem. Sci.* 30:430–436.
9. Heerklotz, H., H. Szadkowska, T. Anderson, and J. Seelig. 2003. The sensitivity of lipid domains to small perturbations demonstrated by the effect of Triton. *J. Mol. Biol.* 329:793–799.
10. Madore, N., K. L. Smith, C. H. Graham, A. Jen, K. Brady, S. Hall, and R. Morris. 1999. Functionally different GPI proteins are organised in different domains on the neuronal surface. *EMBO J.* 19:6917–6926.
11. Gaus, K., M. Rodriguez, K. R. Ruberu, I. Gelissen, T. M. Sloane, L. Kritharides, and W. Jessup. 2005. Domain-specific lipid distribution in macrophage plasma membranes. *J. Lipid Res.* 46:1526–1538.
12. Heffer-Lauc, M., G. Lauc, L. Nimrichter, S. E. Fromholt, and R. L. Schnaar.2005. Membrane redistribution of gangliosides and glycosyl-phosphatidylinositol-anchored proteins in brain tissue sections under conditions of lipid raft isolation. *Biochim. Biophys. Acta.* 1686:200–208.
13. Babiychuk, E. B., and A. Draeger. 2006. Biochemical characterization of detergent-resistant membranes: a systematic approach. *Biochem. J.* 397:407–416.
14. Roper, K., D. Corbeil, and W. B. Huttner. 2000. Retention of prominin in microvilli reveals distinct cholesterol-based lipid micro-domains in the apical plasma membrane. *Nat. Cell Biol.* 2:582–592.
15. Pike, L. J. 2004. Lipid rafts: heterogeneity on the high seas. *Biochem. J.* 378:281–292.
16. Drobnik, W., H. Borsukova, A. Bottcher, A. Pfeiffer, G. Liebisch, G. J. Schutz, H. Schindler, and G. Schmitz. 2002. Apo AI/ABCA1-dependent and HDL3-mediated lipid efflux from compositionally distinct cholesterol-based microdomains. *Traffic.* 3:268–278.
17. Braccia, A., M. Villani, L. Immerdal, L. L. Niels-Christiansen, B. T. Nystrom, G. H. Hansen, and E. M. Danielsen. 2003. Microvillar membrane microdomains exist at physiological temperature. Role of galectin-4 as lipid raft stabilizer revealed by ''superrafts''. *J. Biol. Chem.* 278:15679–15684.
18. Brown, D. A. 2006. Lipid rafts, detergent-resistant membranes, and raft targeting signals. *Physiology* (*Bethesda*). 21:430–439.
19. Hooper, N. M., and A. J. Turner. 1988. Ectoenzymes of the kidney microvillar membrane. Differential solubilization by detergents can predict a glycosyl-phosphatidylinositol membrane anchor. *Biochem. J.* 250:865–869.
20. Brown, D. A., and J. K. Rose. 1992. Sorting of GPI-anchored proteins to glycolipid-enriched membrane subdomains during transport to the apical cell surface. *Cell.* 68:533–544.
21. Ferretti, A., A. Knijn, C. Raggi, and M. Sargiacomo. 2003. High-resolution proton NMR measures mobile lipids associated with Triton-resistant membrane domains in haematopoietic K562 cells lacking or expressing caveolin-1. *Eur. Biophys. J.* 32:83–95.
22. Rinia, H. A., and B. de Kruijff. 2001. Imaging domains in model membranes with atomic force microscopy. *FEBS Lett.* 504:194–199.
23. Lawrence, J. C., D. E. Saslowsky, J. M. Edwardson, and R. M. Henderson. 2003. Real-time analysis of the effects of cholesterol on lipid raft behavior using atomic force microscopy. *Biophys. J.* 84:1827–1832.
24. Rinia, H. A., M. M. Snel, J. P. van der Eerden, and B. de Kruijff. 2001. Visualizing detergent resistant domains in model membranes with atomic force microscopy. *FEBS Lett.* 501:92–96.
25. Morandat, S., and K. El Kirat. 2006. Membrane resistance to Triton X-100 explored by real-time atomic force microscopy. *Langmuir.* 22: 5786–5791.
26. Poole, K., D. Meder, K. Simons, and D. Muller. 2004. The effect of raft lipid depletion on microvilli formation in MDCK cells, visualized by atomic force microscopy. *FEBS Lett.* 565:53–58.
27. Nichols, B. J., A. K. Kenworthy, R. S. Polishchuk, R. Lodge, T. H. Roberts, K. Hirschberg, R. D. Phair, and J. Lippincott-Schwartz. 2001. Rapid cycling of lipid raft markers between the cell surface and Golgi complex. *J. Cell Biol.* 153:529–542.
28. Dukhovny, A., L. Goldstein Magal, and K. Hirschberg. 2006. The MAL proteolipid restricts detergent-mediated membrane pore expansion and percolation. *Mol. Membr. Biol.* 23:245–257.
29. Mayor, S., and F. R. Maxfield. 1995. Insolubility and redistribution of GPI-anchored proteins at the cell surface after detergent treatment. *Mol. Cell. Biol.* 6:929–944.
30. Sharma, P., R. Varma, R. C. Sarasij, Ira, K. Gousset, G. Krishnamoorthy, M. Rao, and S. Mayor. 2004. Nanoscale organization of multiple GPI-anchored proteins in living cell membranes. *Cell.* 116:577–589.
31. Legler, D. F., M.-A. Doucey, P. Schneider, L. Chapatte, F. C. Bender, and C. Bron. 2005. Differential insertion of GPI-anchored GFPs into lipid rafts of live cells. *FASEB J.* 19:73–75.
32. Saslowsky, D. E., J. Lawrence, X. Ren, D. A. Brown, R. M. Henderson, and J. M. Edwardson. 2002. Placental alkaline phosphatase is efficiently targeted to rafts in supported lipid bilayers. *J. Biol. Chem.* 277:26966–26970.
33. Devaux, P. F. 1991. Static and dynamic lipid asymmetry in cell membranes. *Biochemistry.* 30:1163–1173.
34. Zachowski, A. 1993. Phospholipids in animal eukaryotic membranes: transverse asymmetry and movement. *Biochem. J.* 294:1–14.
35. MacDonald, R. I. 1980. Action of detergents on membranes: differences between lipid extracted from red cell ghosts and from red cell lipid vesicles by Triton X-100. *Biochemistry.* 19:1916–1922.
36. Simons, K., and W. L. Vaz. 2004. Model systems, lipid rafts, and cell membranes. *Annu. Rev. Biophys. Biomol. Struct.* 33:269–295.
37. de Almeida, R. F., L. M. Loura, A. Fedorov, and M. Prieto. 2005. Lipid rafts have different sizes depending on membrane composition: a time-resolved fluorescence resonance energy transfer study. *J. Mol. Biol.* 346:1109–1120.
38. London, E. 2005. How principles of domain formation in model membranes may explain ambiguities concerning lipid raft formation in cells. *Biochim. Biophys. Acta.* 1746:203–220.
39. Brugger, B., C. Graham, I. Leibrecht, E. Mombelli, A. Jen, F. Wieland, and R. Morris. 2004. The membrane domains occupied by glycosylphosphatidylinositol-anchored prion protein and Thy-1 differ in lipid composition. *J. Biol. Chem.* 279:7530–7536.
40. Schuck, S., M. Honsho, K. Ekroos, A. Shevchenko, and K. Simons. 2003. Resistance of cell membranes to different detergents. *Proc. Natl. Acad. Sci. USA.* 100:5795–5800.
41. Radeva, G., and F. J. Sharom. 2004. Isolation and characterization of lipid rafts with different properties from RBL-2H3 (rat basophilic leukaemia) cells. *Biochem. J.* 380:219–230.

42. Alfalah, M., G. Wetzel, I. Fischer, R. Busche, E. E. Sterchi, K.-P. Zimmer, H.-P. Sallmann, and H. Y. Naim. 2005. A novel type of detergent-resistant membranes may contribute to an early protein sorting event in epithelial cells. *J. Biol. Chem.* 280:42636–42643.

43. Banerjee, P., A. Dasgupta, B. A. Chromy, and G. Dawson. 1993. Differential solubilization of membrane lipids by detergents: coenrichment of the sheep brain serotonin 5-HT_{1A} receptor with phospholipids containing predominantly saturated fatty acids. *Arch. Biochem. Biophys.* 305:68–77.

44. Hinrichs, J. W., K. Klappe, I. Hummel, and J. W. Kok. 2004. ATP-binding cassette transporters are enriched in non-caveolar detergent-insoluble glycosphingolipid-enriched membrane domains (DIGs) in human multidrug-resistant cancer cells. *J. Biol. Chem.* 279:5734–5738.